JOURNAL OF THE KOREAN ASTRONOMICAL SOCIETY
38: 59 ~ 66, 2005

DEVELOPMENT OF A NEW ION TRANSPORT CODE FOR PLANETARY IONOSPHERES WITH EXPLICIT TREATMENT OF ION-ION COLLISION

YONG HA KIM
Department of Astronomy and Space Science, Chungnam National University, Daejeon 305-764, Korea
E-mail: yhkim@cnu.ac.kr
(Received May 16, 2005; Accepted May 31, 2005)

ABSTRACT

A new ion transport code for planetary ionospheric studies has been developed with consideration of velocity differences among ion species involving ion-ion collision. Most of previous planetary ionosphere models assumed that ions diffuse through non-moving ion and neutral background in order to consolidate continuity and momentum equations for ions into a simple set of diffusion equations. The simplification may result in unreliable density profiles of ions at high altitudes where ion velocities are fast and their velocity differences are significant enough to cause inaccuracy when computing ion-ion collision. A new code solves explicitly one-dimensional continuity and momentum equations for ion densities and velocities by utilizing divided Jacobian matrices in matrix inversion necessary to the Newton iteration procedure. The code has been applied to Martian nightside ionosphere models, as an example computation. The computed density profiles of O^+, OH^+, and HCO^+ differ by more than a factor of 2 at altitudes higher than 200 km from a simple diffusion model, whereas the density profile of the dominant ion, O_2^+, changes little. Especially, the density profile of HCO^+ is reduced by a factor of about 10 and its peak altitude is lowered by about 40 km relative to a simple diffusion model in which HCO^+ ions are assumed to diffuse through non-moving ion background, O_2^+. The computed effects of the new code on the Martian nightside models are explained readily in terms of ion velocities that were solved together with ion densities, which were not available from diffusion models. The new code should thus be expected as a significantly improved tool for planetary ionosphere modelling.

Key words : PLANETS: Jupiter — Ionosphere: Modelling

I. INTRODUCTION

Classical approach of planetary ionosphere modelling took advantage of simplification that minor ions diffuse through medium consisting of non-moving major ions and neutrals (e.g. Banks and Kockarts, 1973). Densities of ions can then be computed from a second order differential equation, so called diffusion equation, that was derived from consolidation of continuity and momentum equations with an appropriate definition of diffusion coefficient. The diffusion approach is valid and efficient for modelling numerous ions that are chemically active and transported through random collision dominantly with background neutrals at most range of altitudes in planetary ionospheres except high altitudes. At high altitudes, ions become less subject to collision with neutrals but still bound to frequent collision with ions due to Coulomb interaction. Infrequent collision with neutrals causes ion transport velocities generally to increase with altitudes, and thus any process depending on velocity becomes important. Since ion drag force, for example, exerted by ion-ion collision is dependent on relative velocities of colliding ions, ion velocities need to be solved explicitly. Classical diffusion equation cannot treat appropriately ion-ion collision that are dependent on velocities of ion species, however.

Ideally, ion densities in planetary ionospheres should be computed simultaneously with neutral densities, velocities, temperatures, stress tensor, and heat flow vector, by solving, so called 13-moment transport equations (c.f. Schunk and Nagy, 2000). This kind of approach has been extensively used for Earth ionosphere studies and especially in modelling of the thermal polar wind (Schunk, 1988; Blelly et al., 1993). For the Martian thermosphere, Boqueho and Blelly (2005) recently developed multimoment multispecies models. The 13-moment transport equations may be too complicated for planetary ionosphere studies, where insufficient measurement data are available to constrain all the model parameters. Therefore, as next improvement over the simple diffusion approach, a new code is developed in this paper to solve continuity and momentum equations explicitly, and thus to calculate drag forces appropriately among ions due to ion-ion collision especially at high altitudes. The code has been applied to the Martian nightside ionosphere as an example case.

II. DESCRIPTION OF ALGORITHM

Densities and transport velocities of ion species in an ionosphere should satisfy the continuity and momentum equations, respectively. In the vertical direction for steady state, the continuity equation for ion species, i, can be written as,

$$f_i^c = \frac{d\phi_i}{dz} - P_i + L_i = 0, \quad (1)$$

where ϕ_i, P_i, and L_i are the flux, production rate, and loss rate of the ion. The momentum equation can be expressed in terms of a vertical ion flux, ϕ_i as

$$f_i^w = \phi_i + D_i(\frac{dn_i}{dz} + \frac{n_i}{H_i}) - n_i w_i^c = 0, \quad (2)$$

where D_i and H_i are a diffusion coefficient and scale height, respectively. Vertical velocity contribution from ion-ion collision, w_i^c, is included in the momentum equation as

$$w_i^c = \frac{\Sigma_{i\neq j}\nu_{ij}w_j}{\Sigma_j\nu_{ij} + \nu_{in}} \equiv \Sigma\alpha_{ij}n_j w_j, \quad (3)$$

where ν_{ij} and ν_{in} are collision frequencies between ion species i and j, and between ion species i and neutrals, and w_j is the vertical velocity of ion species, j (Banks and Kockarts, 1973). The velocity, w_i^c, has a meaning of weighted average velocities of other ions with ion-ion collision frequencies.

The diffusion coefficient can be expressed as

$$D_i = \frac{kT_i/m_i}{\Sigma_j\nu_{ij} + \nu_{in}}, \quad (4)$$

where k, T_i and m_i are the Boltzmann constant, ion temperature, and mass of ion species, i, respectively. The ion-ion collision frequency, ν_{ij}, originates from the Coulomb interaction between ion species i and j, and is given as,

$$\nu_{ij} = \frac{n_j\mu_{ij}^{1/2}(Z_iZ_j)^2}{6.5\times10^7\gamma}\frac{kT_i^{-3/2}}{m_i}, \quad (5)$$

where μ_{ij}, Z_i, Z_j are the reduced mass in atomic unit, charges of ion species i, and j in atomic unit, and γ is a correction factor of 1.5 (Banks and Kockarts, 1973). The scale hight is defined as

$$\frac{1}{H_i} = \frac{m_i g}{kT_i} + \frac{T_e/T_i}{n_e}\frac{dn_e}{dz} + \frac{1}{T_i}\frac{d}{dz}(T_e + T_i), \quad (6)$$

where g, n_e, and T_e are the gravity, electron density and electron temperature, respectively. The electron density is equal to the sum of ion densities at each altitude, $n_e(z) = \Sigma_j n_j(z)$.

In most of ion diffusion transport codes used in planetary ionosphere research, the ion velocity contribution, w_i^c, has not been included, with a simplifying assumption that the ions diffuse through major ions at rest. This simplification allowed the continuity and momentum equations for ion species to be consolidated into a second order differential equation for the ion density, n_i. In reality, major ions diffuse through background neutrals with significant speeds that may affect transport of other ions through the ion-ion collision process. To explore the effect of velocity differences among ions in the ion-ion collision process, the equations (1) and (2), thus, need to be solved explicitly for n_i and ϕ_i $(=n_iw_i)$ or w_i of all ion species at all altitudes of interest.

The first order differential equations (1) and (2) can be expressed numerically by applying forward and backward differencing scheme as

$$f_i^c = \frac{\phi_i(z_{n+1}) - \phi_i(z_n)}{\Delta z} - P_i(z_n) + L_i(z_n), \quad (7)$$

$$f_i^w = \phi_i(z_n) + D_i(z)[\frac{n_i(z_n) - n_i(z_{n-1})}{\Delta z} + \frac{n_i(z_n) + n_i(z_{n-1})}{2H_i(z_n)}] - n_i(z_n)w_i^c(z_n), \quad (8)$$

The difference equations can be solved with Newton iteration method by expressing a large matrix equation, namely,

$$\mathbf{J}\left(\frac{\partial(f_i^c, f_i^w)}{\partial(n_j, \phi_j)}\right)(\widetilde{\delta n_i, \delta\phi_i}) = -(\widetilde{f_i^c, f_i^w}), \quad (9)$$

where the Jacobi matrix $\mathbf{J}$ is a (2× number of species × number of altitude grids) by (2× number of species × number of altitude grids) tridiagonal block matrix. $(\widetilde{\delta n_i, \delta\phi_i})$ is the variation vector of densities and fluxes with a dimension of 2× number of species × number of altitude grids.

The appropriate boundary conditions may be set with $n_i(z_o)$ at the lower boundary, and $\phi_i(z_t)$ at the top boundary. For the first altitude, z_1 above the lower boundary, the equation (9) is then specifically expressed as

$$A_{11}X_1 + A_{12}Y_1 + B_{12}Y_2 = U_1, \quad (10)$$

$$A_{21}X_1 + A_{22}Y_1 = V_1, \quad (11)$$

where X_1 and Y_1 are variation vectors, (δn_i), $(\delta\phi_i)$ of ion densities and fluxes at z_1. U_1 and V_1 are vectors of -f_i^c's and -f_i^w's at z_1. The Jacobi matrix for the first altitude grid can be divided into,

$$A_{11} = \frac{\partial f_i^c}{\partial n_j(z_1)} = -\frac{\partial}{\partial n_j(z_1)}(P_i(z_1) - L_i(z_1)), \quad (12)$$

$$A_{12} = \frac{\partial f_i^c}{\partial\phi_j(z_1)} = -\frac{1}{\Delta z}\delta_{ij}, \quad (13)$$

$$A_{21} = \frac{\partial f_i^w}{\partial n_j(z_1)} = D_i(z_1)(\frac{\delta_{ij}}{\Delta z} + \frac{0.5\delta_{ij}}{H_i(z_1)} + 0.5n_i(z_1)\frac{\partial}{\partial n_j(z_1)}(\frac{1}{H_i(z_1)})) - w_i^c(z_1), \quad (14)$$

$$A_{22} = \frac{\partial f_i^w}{\partial \phi_j(z_1)} = \delta_{ij} - n_i(z_1)\alpha_{ij}, \quad (15)$$

$$B_{12} = \frac{\partial f_i^c}{\partial \phi_j(z_2)} = \frac{\delta_{ij}}{\Delta z}, \quad (16)$$

where δ_{ij} is the unit diagonal matrix. Note that $B_{11} = \frac{\partial f_i^c}{\partial n_j(z_2)}$, $B_{21} = \frac{\partial f_i^w}{\partial n_j(z_2)}$, and $B_{22} = \frac{\partial f_i^w}{\partial \phi_j(z_2)}$ are all null matrices.

For the altitudes, $z_n, n \leq t-2$, up to one grid below the top boundary, the equation (8) can be specifically expressed as

$$A_{11}X_n + A_{12}Y_n + B_{12}Y_{n+1} = U_n, \quad (17)$$

$$C_{21}X_{n-1} + A_{21}X_n + A_{22}Y_n = V_n, \quad (18)$$

where

$$C_{21} = \frac{\partial f_i^w}{\partial n_j(z_{n-1})} = D_i(z_n)(\frac{-\delta_{ij}}{\Delta z} + \frac{0.5\delta_{ij}}{H_i(z_n)} + 0.5n_i(z_n)\frac{\partial}{\partial n_j(z_{n-1})}(\frac{1}{H_i(z_n)})), \quad (19)$$

Also note that $C_{11} = \frac{\partial f_i^c}{\partial n_j(z_{n-1})}$, $C_{12} = \frac{\partial f_i^c}{\partial \phi_j(z_{n-1})}$, and $C_{22} = \frac{\partial f_i^w}{\partial \phi_j(z_{n-1})}$ are all null matrices.

At the last altitude below the top boundary, z_{t-1}, the equation (9) becomes

$$A_{11}X_{t-1} + A_{12}Y_{t-1} + B_{12}Y_t = U_{t-1}, \quad (20)$$

$$C_{21}X_{t-2} + A_{21}X_{t-1} + A_{22}Y_{t-1} = V_{t-1}, \quad (21)$$

When flux boundary condition is applied at the top boundary, $Y_t = \delta\phi = 0$ should be satisfied. The condition for X_t can be found from the difference equation for the momentum equation at z_t as

$$X_t = \frac{D_i(z_t)(1/\Delta z - 0.5/H_i(z_t))}{D_i(z_t)(1/\Delta z + 0.5/H_i(z_t)) - w_i^c}X_{t-1}, \quad (22)$$

This flux boundary condition forces ion densities at the top to be related to those one altitude grid below as

$$n_i(z_t) = \frac{D_i(z_t)(1/\Delta z - 0.5/H_i(z_t))n_i(z_{t-1}) - \phi_i(z_t)}{D_i(z_t)(1/\Delta z + 0.5/H_i(z_t)) - w_i^c}, \quad (23)$$

Once $n_i(z_t)$'s are obtained for the next iteration, $w_i(z_t)$'s are computed from $\phi_i(z_t)/n_i(z_t)$, and are used to calculate $w_i^c(z_t)$'s for the next iteration.

The matrix equations (10), (11), (17), (18), (20), and (21) can be solved for X_n and Y_n, $n = 1 \sim t-1$, with the Gaussian elimination method. In the next iteration, densities and fluxes of ions at all the altitudes ($n = 1 \sim t$) are updated by adding X_n and Y_n to $n_i(z_n)$ and $\phi_i(z_n)$. The iteration continues until $X_n/n_i(z_n)$ and $Y_n/\phi_i(z_n)$ for $n = 1 \sim t-1$ reach less than a convergence criterion of 10^{-3}. In an example case of Martian nightside ionosphere models, the convergence criterion is reached in about 200 iterations.

III. RESULTS AND DISCUSSION

The new code has been used to construct a Martian nightside ionosphere model, which has 18 ions, CO_2^+, Ar^+, N_2^+, O^+, OH^+, N_2H^+, CO^+, C^+, N^+, O_2^+, NO^+, HCO^+, HCO_2^+, H^+, He^+, $O(^2D)^+$, $O(^2P)^+$, O^{++} and 9 neutrals, NO, N, $N(^2D)$, $N(^2P)$, C, $O(^1D)$, $O(^1S)$, H, and H_2. The chemical reactions in the model are mostly from Fox and Sung (2001)'s Venus model, but reactions of OH^+, N_2H^+, HCO^+, HCO_2^+, O^{++} are newly implemented. The added reactions and other details of the Martian nightside model are presented in Kim and Fox (2005).

As a background atmosphere model to the nightside ionosphere, thermospheric densities and temperature are adopted from Bougher and Engel (1999)'s Martian Thermosphere General Circulation Model (MTGCM) for both solar maximum and minimum conditions at 5 am near the equator. The MTGCM computes densities of CO_2, CO, O, N_2, Ar, O_2 and neutral temperatures, which are available to us in the altitude range of 100 - 250 km and 100 - 225 km for solar maximum and minimum, respectively. We utilize the MTGCM species as background neutrals of our model by extrapolating the MTGCM densities and temperature to our model altitude range of 80 - 400 km. We add He as a background neutral by computing its density profile with a mixing ratio of 4×10^{-6} [CO_2] at 80 km from Krasnopolsky and Gladstone (1996) and eddy diffusion coefficients of $6\times 10^7(5\times10^{10}/n)^{0.5}$ cm^2s^{-1} that was found to fit the MTGCM densities of chemically non-active N_2 and Ar with our 1-D diffusion transport model. Fig. 1 shows the background neutral densities and temperatures for solar minimum condition at 5 am near equator. The exospheric temperatures of MTGCM at the night time of 5 am are 156 K and 140 K for solar maximum and minimum, respectively, which are significantly lower than during the daytime. Ion and electron temperatures were provided by J. Fox (private communicaion, 2003). Fig. 1 also shows densities of chemically active neutrals that were computed together with ionospheric species.

At the lower boundary of the model, the densities of ions and neutrals except H and H_2 are assumed to be values of photochemical equilibrium, which are close to zero at the night side. The mixing ratios of 2.0×10^{-7} and 1.5×10^{-5} for H and H_2, respectively, are adopted from Krasnopolksy (2002). At the upper boundary, we consider O_2^+ and O^+ as primary ions being transported from the dayside ionosphere to the nightside. The trans-terminator flux for O_2^+ and O^+ have been computed in Ma et al.(2002)'s 3-D magnetohydrodynamic model. We adopted the downward fluxes, 3×10^7 $cm^{-2}s^{-1}$ and 3.6×10^6 $cm^{-2}s^{-1}$ of O_2^+ and O^+ , which were estimated by assuming that Ma et al's trans-terminator fluxes spread uniformly over the nightside hemisphere. Zero fluxes were assumed for other ions and neutrals that can be subsequently produced from

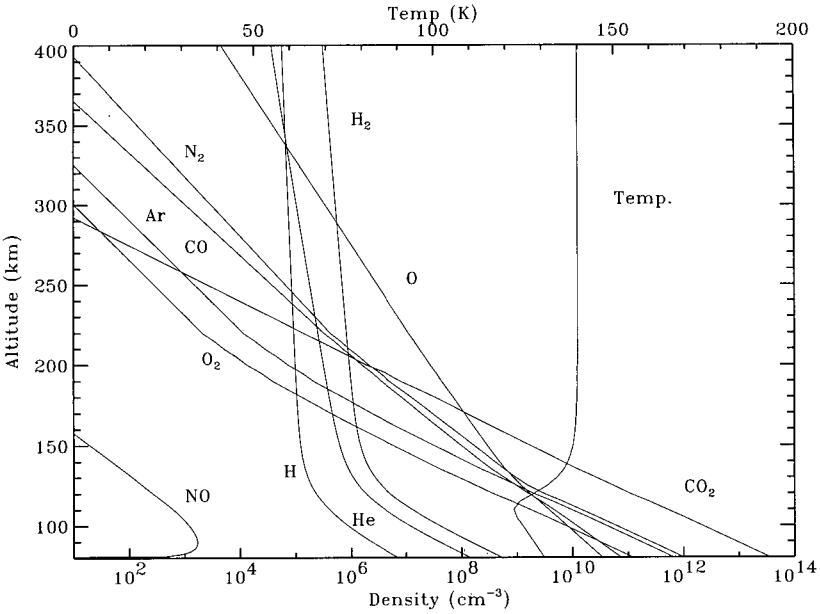

Fig. 1.— Density profiles of background neutral species and temperatures, based on Martian Thermospheric General Circulation Model, for solar manimum condition at 5 AM near equator. Neutral species computed in our nightside ionospheric model are also shown.

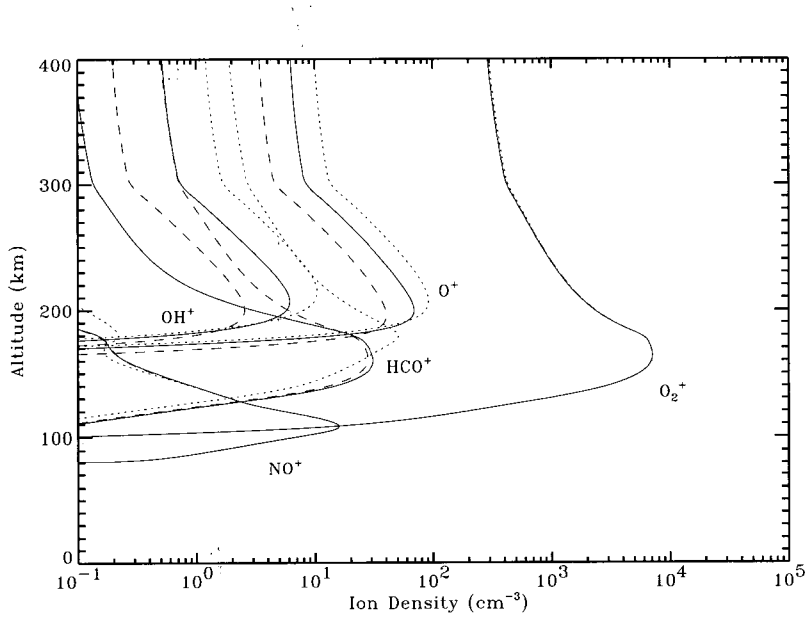

Fig. 2.— Density profiles of ions in the nightside ionosphere. Solid lines are for the model in which different ion velocities are consistently taken into account in the ion-ion collision process. Dotted lines are for the model in which ions are assumed to diffuse through other ions at rest in the ion-ion collision process ($w_i^c = 0$). Dashed lines are for the model in which ions diffuse through only neutrals without the ion-ion collision process ($\nu_{ij} = 0$). Downward fluxes of -3.$\times 10^7$ and -1.8$\times 10^6$ $cm^{-2}s^{-1}$ for O_2^+ and O^+ are assumed at the top boundary.

reactions of the primary ions, O_2^+ and O^+.

Fig. 2 shows density profiles of 5 most populous ions in the nightside ionosphere, computed for the solar minimum condition with downward fluxes with -3.$\times 10^7$ and -1.8$\times 10^6$ cm^{-2}s^{-1} for O_2^+ and O^+. Solid lines are for the fully consistent model in which different ion velocities are solved and taken into account in the ion-ion collision process. Dotted lines are for the model in which ions are assumed to diffuse through other ions at rest in the ion-ion collision process ($w_i^c = 0$). Dashed lines are for the model in which ions diffuse through only neutrals without the ion-ion collision process ($\nu_{ij} = 0$).

As expected from the source fluxes at the top, O_2^+ is the dominant ion with a peak density of 7.1$\times 10^3$ cm^{-3} at 164 km, and O^+ is also a major ion with a peak density of 69 cm^{-3} at 200 km for the consistent model (solid line). Note that O_2^+ density profiles are nearly the same for all three models, whereas O^+ profiles are significantly different among the three models despite the same downward flux assumed at the top boundary. The models with assumptions, $\nu_{ij} = 0$ and $w_i^c = 0$, have resulted in less (dashed line) and greater (dotted line) O^+ densities by about a factor of 2 at most altitudes than the consistent model, respectively. When the ion-ion collision process is completely neglected in ion diffusion process ($\nu_{ij} = 0$), O^+ ions move downward faster due to no drag from the dominant ion O_2^+ and then to be more swiftly converted into other ions, such as OH^+ and HCO^+ at low altitudes, resulting in less densities. On the other hand, when ions are assumed to collide with other ions at rest ($w_i^c = 0$), O^+ ions diffuse downward more slowly due to increased drag from O_2^+ ions at rest than from O_2^+ ions moving downward, resulting in greater densities before conversion into other ions at low altitudes.

In Fig. 2, the O^+ density profile decreases rapidly, as the altitude decreases below its peak, where frequent reaction of O^+ with the dominant background neutral, CO_2, produces O_2^+, contributing to the O_2^+ peak at lower altitudes. Despite no NO^+ input at the top, NO^+ ions are produced mainly by reaction between O_2^+ and NO, and are not lost efficiently due to no reaction with major neutrals, resulting in a significant peak density of 16 cm^{-3} for all three models. Both OH^+ and HCO^+ ions are produced in a series of reactions starting from the primary O^+ ions,

$$O^+ + H_2 \rightarrow OH^+ + H, \qquad (R1)$$

$$OH^+ + CO_2 \rightarrow HCO_2^+ + O, \qquad (R2)$$

$$HCO_2^+ + O \rightarrow HCO^+ + O_2, \qquad (R3)$$

However, HCO^+, being a terminal ion, is lost mainly by recombination,

$$HCO^+ + e \rightarrow CO + H, \qquad (R4)$$

thus accumulating for a longer lifetime than OH^+ to a peak density greater than that of OH^+. Since the ultimate source of HCO^+ and OH^+ is the reaction (R1), their densities depend heavily on the H_2 mixing ratio of the Martian thermosphere. Other ions have densities less than 1 cm^{-3}, and thus not shown in Fig. 2.

Fig. 3 presents velocity profiles of O_2^+ and O^+ ions for the three models. The downward velocities of both O_2^+ and O^+decrease monotonically from maximum values at the top, where both ions are fed into the nightside ionosphere, to nearly zero speed at the lower altitudes, where ion-neutral chemistry takes over diffusion in the continuity equation (eq. 1). The velocity profiles of O_2^+, being the dominant ions, are hardly changed among the three models, whereas those of O^+, affected mostly by the dominant ion O_2^+, vary conspicuously with the different assumption regarding the ion-ion collision process. Downward velocities of O^+ are greatest for the model without ion-ion collision (dashed line) due to no drag from other ions. The least downward velocities (dotted line) are for the model with the assumption of $w_i^c = 0$, which can be explained by the fact that O^+ ions have to move downward against non-moving background ions, especially the dominant ion, O_2^+.

The density profiles of OH^+ and HCO^+ shown in Fig. 2 are greatly affected by the assumption regarding the ion-ion collision process. Although both ions are produced mainly from O^+, changes in their density profiles can be understood with their velocity modification by the given ion-ion collision assumption. Due to the same reason as for O^+ ions, OH^+ ions move downward more slowly or faster after their creation from reaction (R1) for the model with $w_i^c = 0$ or for the model with $\nu_{ij} = 0$ than the consistent model, resulting in the OH^+ density profile changes in Fig. 2. Fig. 4 shows the velocity profiles of OH^+ for the model with $w_i^c = 0$ (dotted line), the model with $\nu_{ij} = 0$ (dashed line), and the consistent model (solid line). However, the HCO^+ density profiles for both non-consistent models indicate greater densities at upper altitudes than for the consistent model. This can be understood in terms of HCO^+ velocity profiles provided in Fig. 5, where the notation are the same as Fig. 4. The HCO^+ ions in the consistent model move downward at the fastest speed, and thus their densities are the least among the three models. Unlike O^+ and OH^+ ions, HCO^+ ions that are produced from serial reactions, (R1), (R2), (R3), at relatively lower altitudes, are swept downward by the downward moving dominant O_2^+ ions via ion-ion collision in the consistent model. For the non-consistent models, the HCO^+ ions move downward with slower speed either due to no momentum gain ($\nu_{ij} = 0$) or due to drag ($w_i^c = 0$) from the dominant O_2^+ ions, resulting in greater densities at high altitudes.

IV. CONCLUSIONS

A new ion transport code has been developed for planetary ionosphere modelling with an intention to in-

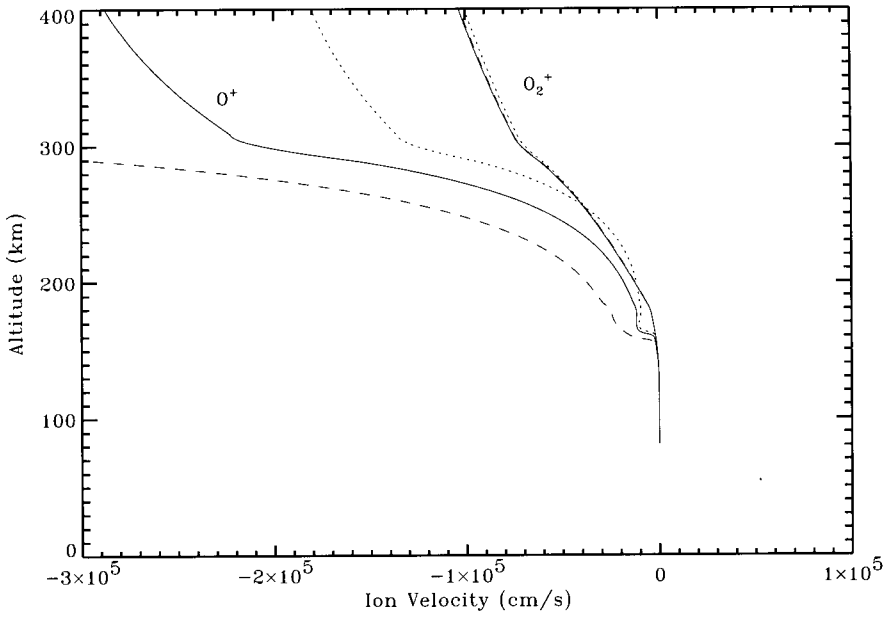

Fig. 3.— Velocity profiles of O_2^+ and O^+ in the nightside ionosphere. Solid lines are for the model with ion-ion collision process consistently included, dotted lines are for the model with $w_i^c = 0$ and dashed lines are for the model without the ion-ion collision process ($\nu_{ij} = 0$). Note that velocities of O_2^+ , the major ion, show very little differences among the models, while downward velocities of O^+ change greatly at high altitudes.

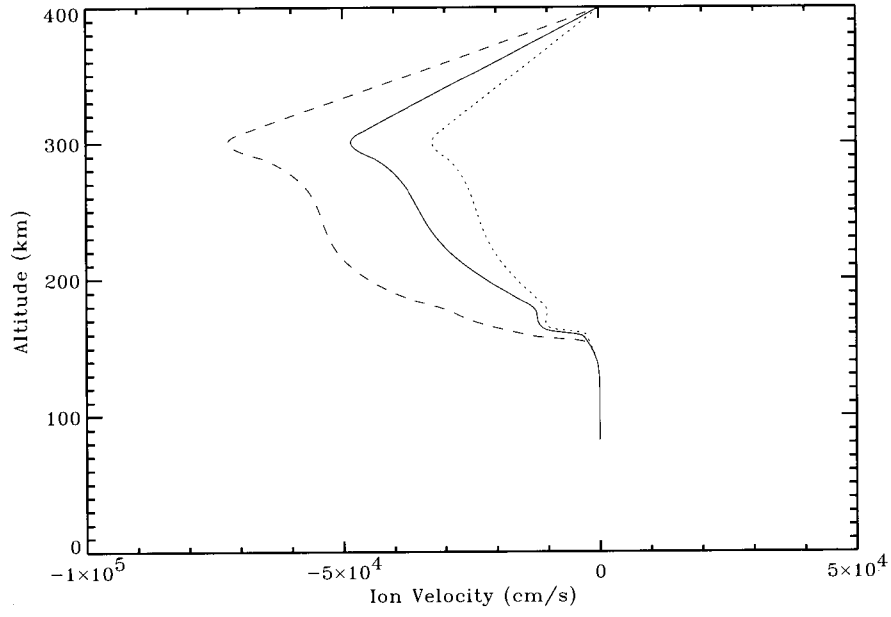

Fig. 4.— Velocity profiles of OH^+ in the nightside ionosphere. Notation is the same as in Fig. 3. Note that velocities change greatly at most altitudes except near the top boundary where the velocity was fixed to be zero as a boundary condition.

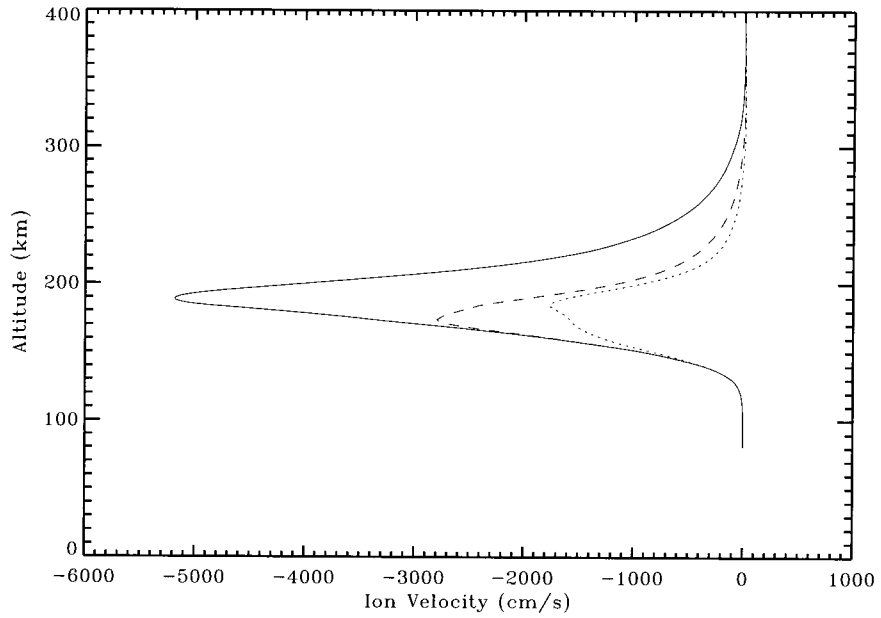

Fig. 5.— Velocity profiles of HCO^+ in the nightside ionosphere. Notation is the same as in Fig. 3. Note that downward velocities for the consistent model are greatest among the three models because HCO^+ ions produced at relatively low altitudes are swept by the downward moving dominant O_2^+ ions via ion-ion collision.

clude consistently the effect of ion-ion collision among ions that move significantly fast relative each other. Most of previous planetary ionosphere models utilized the diffusion equation derived from consolidation of continuity and momentum equations with a simplifying assumption that ions either do not collide with other ions or collide with other ions at rest. The simplification may cause unreliable densities of ions especially at high altitudes, where ion velocities are fast and their velocity differences influence significantly the effect of ion-ion collision. A new code solves explicitly one-dimensional continuity and momentum equations for ion densities and velocities by utilizing divided Jacobian matrices when inverting the Jacobi matrix, necessary to the Newton iteration procedure. By applying the new code to Martian nightside ionosphere models, I find that the densities of O^+, OH^+, and HCO^+ differ by more than a factor of 2 at altitudes higher than 200 km from a simple diffusion model, whereas the density profile of the dominant ion, O_2^+, changes little. Especially, the densities of HCO^+ are reduced by a factor of about 10 and its peak altitude is lowered by about 40 km from a simple diffusion model in which HCO^+ ions are assumed to diffuse through non-moving ion background, O_2^+. The computed differences from the new code in the Martian nightside models are understood readily in terms of ion velocities, which were not available from diffusion models. The new code should thus be expected as an improved tool for planetary ionosphere modelling.

ACKNOWLEDGEMENTS

YHK acknowledges the financial support of the Korea Research Foundation (KRF-2003-013-C00043).

REFERENCES

Bank, P. M., & G. Kockarts, 1973, Aeronomy Part B., Academic Press, New York, 163

Blelly, P.-L. D. Alcayde, M. Blanc, & J. Fontanari, 1993, Thermal polar wind: Opportunities with the EISCAT Svalbard radar, Ann. Geophys., 10, 498-510

Boqueho, V., & P.-L. Blelly, 2005, Contributions of a multimoment multispecies approach in modeling planetary atmospheres: Example of Mars, J. Geophys. Res., 110, A01313

Bougher, S. W., & S. Engel, 1999, Comparative terrestrial planet thermospheres 2. Solar cycle variation of global structure and winds at equinox, J. Geophys. Res., 104, 16,591

Fox, J. L., & K. Y. Sung, 2001, Solar activity variations of the Venus thermosphere/ionosphere, J. Geophys. Res., 106, 21,305-21,335

Kim, Y. H., & J. L. Fox, 2005, The nightside ionosphere of Mars: Limits sustainable by plasma transport from the dayside ionosphere, in preparation

Krasnopolsky, V. A., & G. R. Gladstone, 1996, Helium on Mars: EUVE and Phobos data and implications for Mars' evolution, J. Geophys. Res., 101, 15, 765–15772

Krasnopolsky, V. A., 2002, Mar's upper atmosphere and ionosphere at low, medium, and high solar activities: Implications for evolution of water, J. Geophys. Res., 107, 5128

Ma, Y., A. F. Nagy, K. C. Hansen, D. L. DeZeeuw, & T. I. Gombosi, 2002, Three-dimensional multispecies MHD studies of the solar wind interaction with Mars in the presence of crustal fields, J. Geophys. Res., 107, 1282

Schunk, R. W., 1988, The Polar Wind, AGU, Washington D.C., 219-228

Schunk, R. W., & A. Nagy, 2000, Ionospheres: Physics, Plasma Physics, and Chemistry, Cambridge Univ. Press, Cambridge, 59-63